PERSIANN-CDR

Daily Precipitation Climate Data Record from Multisatellite Observations for Hydrological and Climate Studies

by Hamed Ashouri, Kuo-Lin Hsu, Soroosh Sorooshian, Dan K. Braithwaite, Kenneth R. Knapp, L. Dewayne Cecil, Brian R. Nelson, and Olivier P. Prat

Developing the PERSIANN-CDR rainfall estimation algorithm and applying it to historical multisatellite observations produces a long-term dataset that can be used to study the water cycle at higher resolutions than previously possible.

L ong-term global precipitation observations are of primary importance for climate studies. Proper observations are needed for sustainable global-scale monitoring of precipitation variability and trends in space and time at resolutions suitable

AFFILIATIONS: Ashouri, Hsu, Sorooshian, and Braithwaite—Center for Hydrometeorology and Remote Sensing, Henry Samueli School of Engineering, Department of Civil and Environmental Engineering, University of California, Irvine, Irvine, California; Knapp and Nelson—NOAA/National Climatic Data Center, Asheville, North Carolina; Cecil—Global Science & Technology, Inc., Asheville, North Carolina; Prat—Cooperative Institute for Climate and Satellites, North Carolina State University, and NOAA/National Climatic Data Center, Asheville, North Carolina

CORRESPONDING AUTHOR: Hamed Ashouri, Center for Hydrometeorology and Remote Sensing, Department of Civil and Environmental Engineering, University of California, Irvine, CA 92697
E-mail: h.ashouri@uci.edu

for climate studies (e.g., Solomon et al. 2007; Wentz et al. 2007). There are various other sources of rainfall information. Ground-based rain gauge networks are one of the most widely used sensors to measure precipitation. The longest historical precipitation observations are available through rain gauge records (Xie et al. 2003). A significant number of climate studies have focused on precipitation analysis using historical observational data (e.g., Karl et al. 1995 and Higgins et al. 2007, among many others). Although gauges can directly measure the rain that reaches the ground surface, they are land based, sparse, and point measurements. Therefore, gauge observations are insufficient for the development of a reliable high-resolution global dataset. Radar and satellite are two other data sources that can provide a viable alternative to gauge measurement for developing high-resolution estimates of precipitation in global scale. Radar data are a great source of high-resolution precipitation estimates (Lin and Mitchell 2005); however, the data are not available wherever the radar coverage is poor and the radar beam is blocked (Westrick et al. 1999; Maddox et al. 2002). Satellite observations, however, have more complete converge, particularly over oceans, high altitudes, and remote regions where gauge measurements are very limited or unavailable.

Geostationary Earth orbiting (GEO) satellites are capable of providing images every 15–30 min in multiple spectral bands of the cloud patterns and evolution over time. GEO infrared (IR)-based algorithms are considered to be effective at identifying tropical convective systems in both day and night, but the performance of an IR-based algorithm is less accurate for warm rain clouds and cold high cirrus, nonraining clouds. Passive/active microwave (PMW) sensors aboard low Earth orbit (LEO) satellites can measure hydrometeor distribution in rain clouds more directly than GEO-based sensors. The low sampling frequency of LEO satellites, however, limits the effectiveness of PMW-based rainfall data retrieval at short time scales. Integration of multiple LEO satellites can improve this sampling limitation and as a result improve precipitation estimation at short time scales considerably.

Development of global satellite-based precipitation datasets has been an emerging research area in the past three decades. Since 1997, the Tropical Rainfall Measurement Mission (TRMM) has improved rainfall retrievals over the tropical regions (Kummerow et al. 1998; Simpson et al. 1988; Kummerow et al. 2000). The Global Precipitation Measurement (GPM) mission, which was launched in 27 February 2014, combines observations from multiple microwave (MW) sensors on LEO satellites to provide information on global precipitation distributions in 3-h periods (Hou et al. 2008, 2014). The Global Precipitation Climatology Project (GPCP; Huffman et al. 1997; Huffman et al. 2001; Adler et al. 2003) and the Climate Prediction Center (CPC) Merged Analysis of Precipitation (CMAP; Xie and Arkin 1997; Xie et al. 2003) are two other datasets with long records of data. These datasets, with their global coverage (over oceans and land) and long-term time periods, albeit

at 2.5° and monthly spatiotemporal resolution have contributed greatly to climate change studies (e.g., Yilmaz and DelSole 2010; Allan et al. 2010; Peterson et al. 2012; Bourassa et al. 2013; Ma et al. 2013; Kucera et al. 2013; Rossow et al. 2013). However, their coarse spatial and temporal resolution limits their ability to capture the spatial details and dynamics of extreme precipitation events, particularly hurricanes and convective storms, whose life cycles range from hours to days. Table 1 shows the time coverage and spatiotemporal resolution of current major satellite-based precipitation datasets (the last row shows the specifications of the product that has been developed and presented in this study).

As defined by the World Meteorological Organization (WMO), at least 30 years of historical weather data are generally required for climatological studies (Burroughs 2003). As shown in Table 1, current satellite-based precipitation datasets are either of insufficient duration for climate studies or their temporal and/or spatial resolution is too coarse for analysis of climate extremes. Therefore, development of a global, long-term, high-resolution, satellite-based precipitation dataset is needed. According to the assessment of current global precipitation products by the World Climate Research Programme (WCRP) Global Energy and Water Exchanges (GEWEX), improving and extending the current global precipitation products is identified as the biggest challenge facing the scientific community (Gruber and Levizzani 2008). Moreover, pursuing efforts for obtaining higher spatial and temporal resolution precipitation data is recognized as being of great importance.

Generally, high-resolution, satellite-based precipitation estimation algorithms rely on the synergy between the superior quality, yet infrequent, LEO PMW observations and the high sampling rate of IR

TABLE 1. Coverage and spatiotemporal resolutions of major satellite precipitation products, including PERSIANN-CDR (in bold).

Product	Temporal resolution	Spatial resolution	Period	Coverage
GPCP	Monthly/Pentad	2.5°	1979–(delayed) present	90°S–90°N
GPCP-IDD	Daily	1°	1996–(delayed) present	90°S–90°N
CMAP	Monthly/Pentad	2.5°	1979–(delayed) present	90°S–90°N
TMPA v7	3 hourly	0.25°	1998–(delayed) present	50°S–50°N
CMORPH	0.5 h	~0.07°*	2002–present	60°S–60°N
PERSIANN	0.5 h	0.25°	2000–present	60°S–60°N
PERSIANN-CCS	0.5 h	0.04°	2003–present	60°S–60°N
PERSIANN-CDR	**Daily**	**0.25°**	**1983–(delayed) present**	**60°S–60°N**

* CMORPH resolution is ~8 km.

observations from GEO satellites. Examples of these algorithms and products are the CPC morphing technique (CMORPH; Joyce et al. 2004), Precipitation Estimation from Remotely Sensed Information using Artificial Neural Networks (PERSIANN; Hsu et al. 1997, 1999), TRMM Multi-Satellite Precipitation Analysis (TMPA; Huffman et al. 2007), and the NRL-Blend satellite rainfall estimates from the Naval Research Laboratory (NRL; Turk et al. 2010).

CMORPH produces high-resolution global precipitation analysis based on LEO-based PMW observations from different sources, such as the Defense Meteorological Satellite Program (DMSP) F-13, F-14, F-15 [Special Sensor Microwave Imager (SSM/I)], and F-16 [Special Sensor Microwave Imager/Sounder (SSMI/S)]; the *National Oceanic and Atmospheric Administration (NOAA)-15, -16, -17,* and *-18* [Advanced Microwave Sounding Unit (AMSU)-B]; *Aqua* [Advanced Microwave Scanning Radiometer for the Earth Observing System (AMSR-E)]; and the TRMM Microwave Imager (TMI). Half-hourly CMORPH data at 8-km spatial resolution has been operationally produced since 22 November 2002 (Joyce et al. 2004). PERSIANN primarily uses infrared brightness temperature data from geostationary satellites to estimate rainfall rate, updating its parameters using PMW observations from low-orbital satellites. The PERSIANN half-hourly 0.25° rain-rate product is available for March 2000 to the present (Hsu et al. 1997). The version 7 TMPA data product (Huffman et al. 2007) has 3-hourly and 0.25° temporal and spatial resolution, respectively, starting from January 1998. The TMPA algorithm combines high-quality PMW observations and IR data from geostationary satellites to derive precipitation. The NRL-Blend satellite precipitation dataset is another precipitation product based on both geostationary visible and infrared data and PMW observations (Turk et al. 2010). The NRL global precipitation accumulation product is available at 0.25° and 3-hourly spatiotemporal resolutions starting in January 2004.

As can be seen with the aforementioned products, high-resolution, satellite-based, precipitation estimation algorithms generally need PMW observations as a major source of input data. Such algorithms would be unable to provide reliable precipitation estimates when PMW samples are limited or unavailable. This is particularly the case for the pre-1997 period, when only one or two PMW observations are available daily. This constraint limits the application of these algorithms in the reconstruction of precipitation records during the pre-PMW era necessary for more significant global climate studies.

Among high-resolution, satellite-based, precipitation estimation algorithms, PERSIANN, because of its primary reliance on infrared information that dates back to 1979, is very suitable for estimating historical precipitation over the past three decades. To meet the calibration requirement of PERSIANN, the model is pretrained using the National Centers for Environmental Prediction (NCEP) stage IV hourly precipitation data. Then the parameters of the model are kept fixed, and the model is run for the full historical record of IR data. The archive of global IR data is available through the International Satellite Cloud Climatology Project (ISCCP). To reduce the biases in the PERSIANN-estimated precipitation while preserving the spatial and temporal patterns in high resolution, 2.5° monthly GPCP precipitation data were utilized. The bias-corrected PERSIANN precipitation estimates maintain a monthly total consistent with the monthly GPCP product. The final product, called the PERSIANN-CDR (for Climate Data Record), provides a 30-yr record of near-global (60°S–60°N) daily precipitation data at 0.25° spatial resolution. Consistency of PERSIANN-CDR precipitation data over the entire 30-yr record was maintained throughout the modeling process. All of these characteristics make PERSIANN-CDR a useful product for global climate studies at a scale relevant to extreme weather events.

The scope of this paper is organized as follows: The second section ("Data") presents information regarding the utilized data. The third section ("Methodology") provides a detailed explanation of the methodology. The fourth section ("PERSIANN-CDR product") describes the details of the PERSIANN-CDR product, and the fifth section ("Case studies") details the validation studies of PERSIANN-CDR with three case studies. The last section provides the conclusions.

DATA. *Stage IV precipitation data.* The stage IV precipitation product is made available by the NCEP Environmental Modeling Center (EMC) from high-resolution Doppler next-generation radars (NEXRADs) and hourly rain gauge data over the continental United States. Stage IV data are provided over the 4×4 km² Hydrologic Rainfall Analysis Project (HRAP) national grid system and are made available at hourly, 6-hourly, and 24-hourly scales. The 12 River Forecast Centers (RFCs) of the National Weather Service (NWS) do manual quality control and NCEP further mosaics all the data received from the RFCs. Different studies have investigated the uncertainties associated with stage IV data (Westrick et al. 1999; Young et al. 2000; Maddox et al. 2002;

Young and Brusnell 2008; Habib et al. 2009), and great efforts have been made to improve the quality of the data (Lin and Mitchell 2005). More information about stage IV data can be obtained from Fulton et al. (1998) and from this webpage link: www.emc.ncep.noaa.gov/mmb/ylin/pcpanl/stage4/. This dataset has been widely used as a reference for evaluation of satellite-based precipitation estimations (Ebert et al. 2007; Zeweldi and Gebremichael 2009; Anagnostou et al. 2010; AghaKouchak et al. 2011). In this study, stage IV radar data are used for the initial training the neural network (NN) model as well as evaluating the performance of PERSIANN-CDR.

Gridded satellite infrared data (GridSat-B1). As the custodian of major climate datasets, the NOAA/National Climatic Data Center (NCDC) maintains a historical archive of data from GEO satellites as compiled by the International Satellite Cloud Climatology Project (ISCCP). ISCCP B1 global geostationary observations (Knapp 2008a) comprise all channel observations from a number of international GEO satellites, including the Geostationary Operational Environmental Satellite (GOES) series, the European Meteorological satellite (Meteosat) series, the Japanese Geostationary Meteorological Satellite (GMS) series, and the Chinese Fen-Yung 2 (FY2) series. The ISCCP B1 IR brightness temperature data available from these GEO sources cover the time period from 1979 to the present at space and time resolutions of 10-km and 3-h intervals. Better global coverage began in 1983, albeit with a gap over the Indian Ocean due to a lack of GEO data (Rossow and Schiffer 1991; Rossow and Garder 1993; Knapp 2008a).

Gridded satellite (GridSat-B1) data are derived from merging ISCCP B1 IR data [see Knapp et al. (2011) for complete details]. GridSat-B1 provides near-global data for three channels: visible, infrared window (IRWIN), and infrared water vapor (IRWVP). GridSat-B1 IRWIN data, the main input data to the PERSIANN-B1 model, are merged using the nadirmost observations at each grid point and adjusted for different biases in satellite sensors [see Knapp (2008b) for details regarding intersensor differences]. The infrared window brightness temperature data, GridSat-B1 CDR (Knapp et al. 2011), spans from 1 January 1980 to the current time, covering the globe from 70°S to 70°N and 180°W to 180°E. The GridSat-B1 IRWIN brightness-temperature data are gridded to a 0.07° resolution latitude–longitude grid and are available at a 3-hourly time scale. To make GridSat data compatible with the input structure of the PERSIANN model, these data were averaged and upscaled to a 0.25° resolution and filtered to remove data values out of the normal range for IR data.

Global Precipitation Climatology Project. The Global Precipitation Climatology Project (GPCP) was established in 1986 by the World Climate Research Programme (WCRP) to document the spatial and temporal distribution of precipitation at climate scale (WCRP 1986; Adler et al. 2003). Currently, three GPCP global precipitation products are available (see Table 1): 1) monthly, 2.5° merged analysis (1979–present); 2) pentad, 2.5° merged analysis (1979–present); and 3) 1° daily (1DD) merged analysis (October 1996–present).

The GPCP monthly 2.5° merged analysis was constructed using multisatellite (SSM/I and IR) precipitation estimates, adjusting the latter using gauge analysis to remove large-scale bias, and then merging satellite and gauge analyses into a final product (Huffman et al. 1997, 2001; Adler et al. 2003; Huffman et al. 2009). GPCP monthly rainfall includes precipitation gauge analysis provided by the Global Precipitation Climatology Centre (GPCC; Rudolf 1993, Rudolf et al. 1994; Schneider et al. 2008). The existing long-term monthly GPCP product has been widely used for climatology studies on a global scale. In this study, the latest version of the GPCP monthly 2.5° product (version 2.2) was used for correcting the biases of the PERSIANN rain-rate estimates. GPCP version 2.2 is available at http://precip.gsfc.nasa.gov and currently spans January 1979 to November 2012. Documentation of the GPCP version 2.2 is accessible at http://www1.ncdc.noaa.gov/pub/data/gpcp/gpcp-v2.2/doc/.

In addition to the monthly product, the GPCP 1° daily precipitation product (Huffman et al. 2001) was used for evaluation purposes. GPCP 1DD documentation is available at http://www1.ncdc.noaa.gov/pub/data/gpcp/1dd-v1.1/1DD_v1.1_doc.pdf.

METHODOLOGY. The development of the PERSIANN-CDR precipitation product is aimed at addressing the need for a consistent, long-term, high-resolution near-global dataset to study the spatial and temporal characteristics of precipitation in a scale relevant to climate studies. In this study, the PERSIANN algorithm is applied to the historical archive of GridSat-B1 infrared window observations from GEO satellites to generate 3-hourly rain-rate estimates (1980–2012) at 0.25° for the region between 60°S and 60°N. To be consistent throughout this paper, the output from the PERSIANN model using GridSat-B1 data with no PMW training and no bias correction is called PERSIANN-B1. The GPCP monthly product is then used to remove the biases of the PERSIANN-B1 rain-rate estimates,

making it consistent with the GPCP monthly product. Adjusted PERSIANN-B1 rain-rate estimates resulting from this stage are represented as Adj_$r_{\text{PERSIANN·B1}}$ in this paper. Last, the 3-hourly Adj_$r_{\text{PERSIANN·B1}}$ precipitation data are accumulated to the daily scale to produce the PERSIANN-CDR product. Detailed information regarding the PERSIANN-CDR algorithm and the bias-adjustment process is presented in the following subsections.

PERSIANN-CDR precipitation estimation algorithm. The existing PERSIANN algorithm provides global precipitation estimates using combined IR and PMW information from multiple GEO and LEO satellites. The algorithm uses an artificial neural network (ANN) model to extract cold-cloud pixels and neighboring features from GEO longwave infrared images (10.2–11.2 μm) and associates variations in each pixel's brightness temperature to estimate the pixel's surface rainfall rate (Hsu et al. 1997, 1999; Sorooshian et al. 2000). The PMW information from LEO satellites and the CPC globally merged, full-resolution (4 km, 1/2 hourly) IR data from GEO satellites (Janowiak et al. 2001) are processed to 0.25° × 0.25° latitude/longitude spatial resolution for rainfall estimation using the PERSIANN model.

In this CDR product, in order to eliminate the need for PMW observations, the nonlinear regression parameters of the ANN model are trained and remain fixed when PERSIANN is used for retrospective estimation of rainfall rates using the 3-hourly GridSat-B1 IRWIN data. Furthermore, a bias-adjustment stage based on GPCP 2.5° monthly precipitation data is incorporated into the reconstruction process. The data-

generation framework incorporates GPCP monthly rainfall data to adjust 3-hourly PERSIANN-B1 rainfall estimates and therefore ensures data consistency and quality. Figure 1 shows a simplified schematic of the current operational PERSIANN-CDR system.

Adjusting daily PERSIANN data using monthly GPCP data. To reduce any biases in the 3-hourly PERSIANN-B1 estimates, while at the same time preserving spatial and temporal patterns in the high-resolution precipitation estimates, GPCP monthly rainfall at 2.5° resolution is used to adjust the high-resolution PERSIANN-B1 estimates. A separate correction is performed for each 2.5° grid box of PERSIANN-B1 data for each month of each year. For each 2.5° (i', j') grid box, the corresponding 0.25° 3-hourly PERSIANN-B1 rain-rate estimates $r_{\text{PERSIANN}-\text{B1}}$ (i, j) are spatially and temporally aggregated to 2.5° monthly scale [$R_{\text{PERSIANN}-\text{B1}}$ (i', j')]. In doing so, a threshold value [thd in Eq. (1)] needs to be applied to the 3-hourly PERSIANN-B1 rain-rate estimates to filter out noisy pixels. These noisy pixels are generally associated with pixels where the rain rate is "zero" but the neural network model estimates a very small nonzero value. While the resulting noisy pixels may not affect the adjustment process considerably, they can lead to a very large number of "rainy" days (rain rate > 0 mm day^{-1}):

$$R_{\text{PERSIANN-B1}}(i', j') = \sum_{}^{nd}\sum_{}^{nh}\left(\sum_{}^{10}\sum_{}^{10}[r_{\text{PERSIANN-B1}}(i, j) \geq \text{thd}]\right). \quad (1)$$

In Eq. (1), i and j are the high-resolution (0.25°) latitude and longitude, i' and j' are the low-resolution (2.5°)
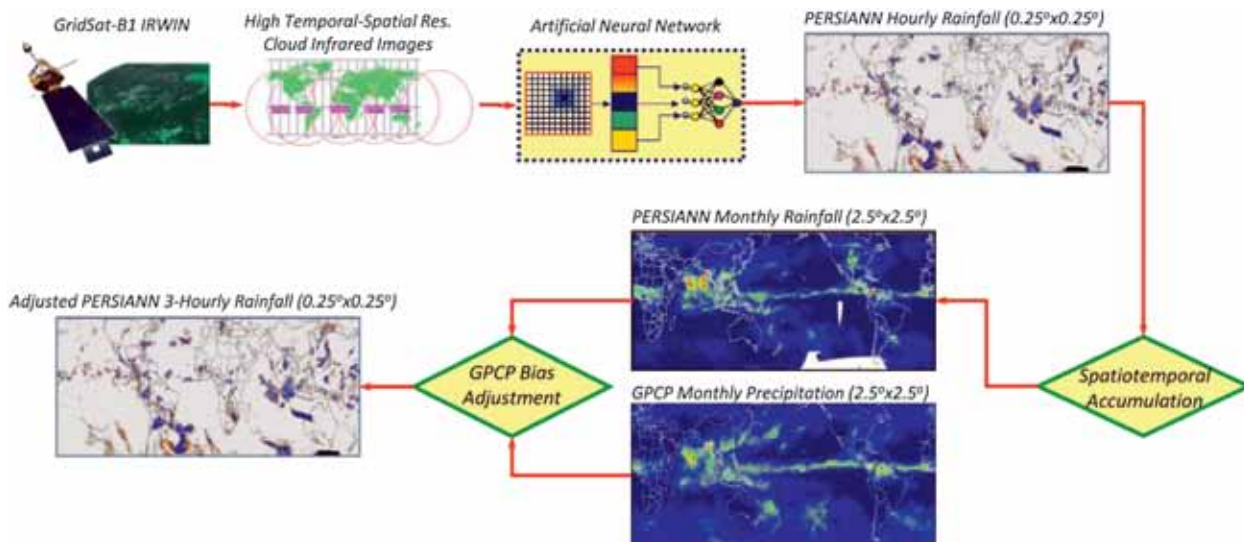

FIG. 1. A schematic of the PERSIANN-CDR algorithm for reconstruction of historical precipitation.

latitude and longitude, nh is the number of 3-hourly PERSIANN-B1 samples in each day, and nd is the number of days in each month. The correction factor for each monthly 2.5° grid cell is then calculated as follows:

$$w(i', j') = R_{GPCP}(i', j') / R_{PERSIANN-B1}(i', j'), \quad (2)$$

where R_{GPCP} is the 2.5° monthly GPCP precipitation for a given pixel. We note that in some locations, such as high latitudes and in dry regions with very low rainfall values, the weight (w) can become large. This can lead to unreasonably large daily rainfalls in finer resolution. To prevent such cases, we applied a cap for the maximum weight. To find the best combination of thd and maximum w, an optimization model was developed with the objective of finding the combination that gives the minimum mean absolute error (MAE) between GPCP-1DD and PERSIANN-CDR (upscaled to 1°). The results show that thd = 0.1 and maximum w = 20 is perhaps the best combination.

The monthly bias is then spatially downscaled and removed from the PERSIANN-B1 estimates at 0.25° resolution using the correction factor. Each 2.5° grid cell covers 10 × 10 pixels of PERSIANN-B1 estimation. To prevent discontinuities at the edges of the 10 × 10 pixels after adjustment, the correction factor $w(i', j')$ is assigned to the center of each 10 × 10 pixel block and then a linear interpolation method is applied to find the correction factor at each 0.25° pixel [$w(i, j)$]. Thus, each 0.25° pixel is corrected with a separate adjustment factor, which results in a smooth and continuous transition over the edge of the 10 × 10 pixels. The GPCP-adjusted 0.25° monthly PERSIANN-B1 precipitation, $Adj\_R_{PERSIANN-B1}(i, j)$, is then calculated as follows:

$$Adj\_R_{PERSIANN-B1}(i, j) = w(i, j) * R_{PERSIANN-B1}(i, j). \quad (3)$$

Because of the linearity of the bias adjustment process, the correction factor can be applied to the higher temporal resolution PERSIANN-B1 estimates. Thus, the GPCP-adjusted 0.25° 3-hourly PERSIANN-B1 precipitation, $Adj\_r_{PERSIANN-B1}$, is calculated as follows:

$$Adj\_r_{PERSIANN-B1}(i, j) = w(i, j) * r_{PERSIANN-B1}(i, j). \quad (4)$$

Equation (4) is applied to each 3-hourly PERSIANN-B1 estimate, which results in distributing the monthly bias correction to the 3-hourly precipitation estimates.
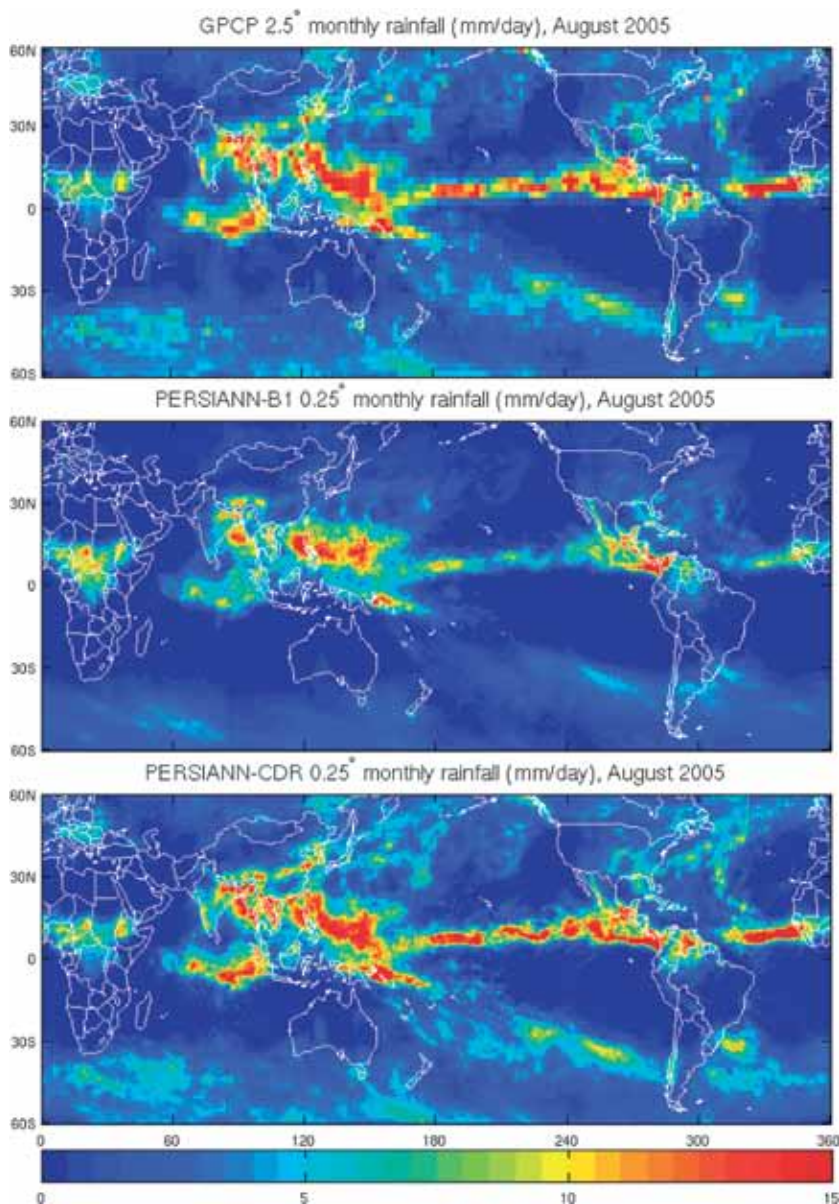

Fig. 2. Global rainfall maps (mm day⁻¹) for August 2005 from (top) GPCP 2.5° (Adler et al. 2003), (middle) PERSIANN-B1 0.25°, and (bottom) PERSIANN-CDR 0.25° monthly datasets.

The bias-adjusted PERSIANN-B1 precipitation data maintains GPCP monthly total precipitation. To reduce uncertainty, the 3-hourly $Adj\_r_{PERSIANN-B1}$ rain-rate data are accumulated to daily scale to produce the PERSIANN-CDR product:

$$PERSIANN-CDR(i,j) = \sum_{n=1}^{N} Adj\_r_{PERSIANN}(i,j,n), (5)$$

where N is the number of $Adj\_r_{PERSIANN-B1}$ samples per day.

PERSIANN-CDR PRODUCT. PERSIANN-CDR is a daily 0.25° precipitation product that covers the area between 60°S and 60°N latitude and 0° and 360° longitude. The current version of the product spans the period 1 January 1983 to 31 December 2012. Work is in progress to complete the years of 1980, 1981, and 1982, where the quality of the GridSat-B1 data for few months of each year needs further improvement. In addition, PERSIANN-CDR will be extended beyond 2012 to near-current time as both GridSat-B1 IR data and GPCP monthly rainfall data become available.

Figure 2 shows the results of the adjustment of PERSIANN-B1 estimates for August 2005 compared to GPCP (Fig. 2, top) before adjustment (Fig. 2, middle) and after adjustment (Fig. 2, bottom). After GPCP adjustment, even by visual comparison, it is clear that there is an improvement of the PERSIANN-CDR estimates toward GPCP estimates.

To investigate whether or not the GPCP precipitation product was properly assimilated into the PERSIANN-CDR product, the mean areal precipitation (MAP) for both the northern and southern tropical regions from monthly PERSIANN-B1, PERSIANN-CDR, and GPCP data were calculated. As shown in Fig. 3, the resulting time series of the mean areal precipitation from PERSIANN-CDR matches well with that of GPCP monthly product.

PERSIANN-CDR was also compared with GPCP-1DD in daily scale. Mean areal precipitation estimates for different regions of the globe for daily PERSIANN-B1, PERSIANN-CDR, and GPCP-1DD were calculated. The result over the whole globe for the period of 2007–09 is shown in Fig. 4. Improvements become evident after applying the bias-adjustment
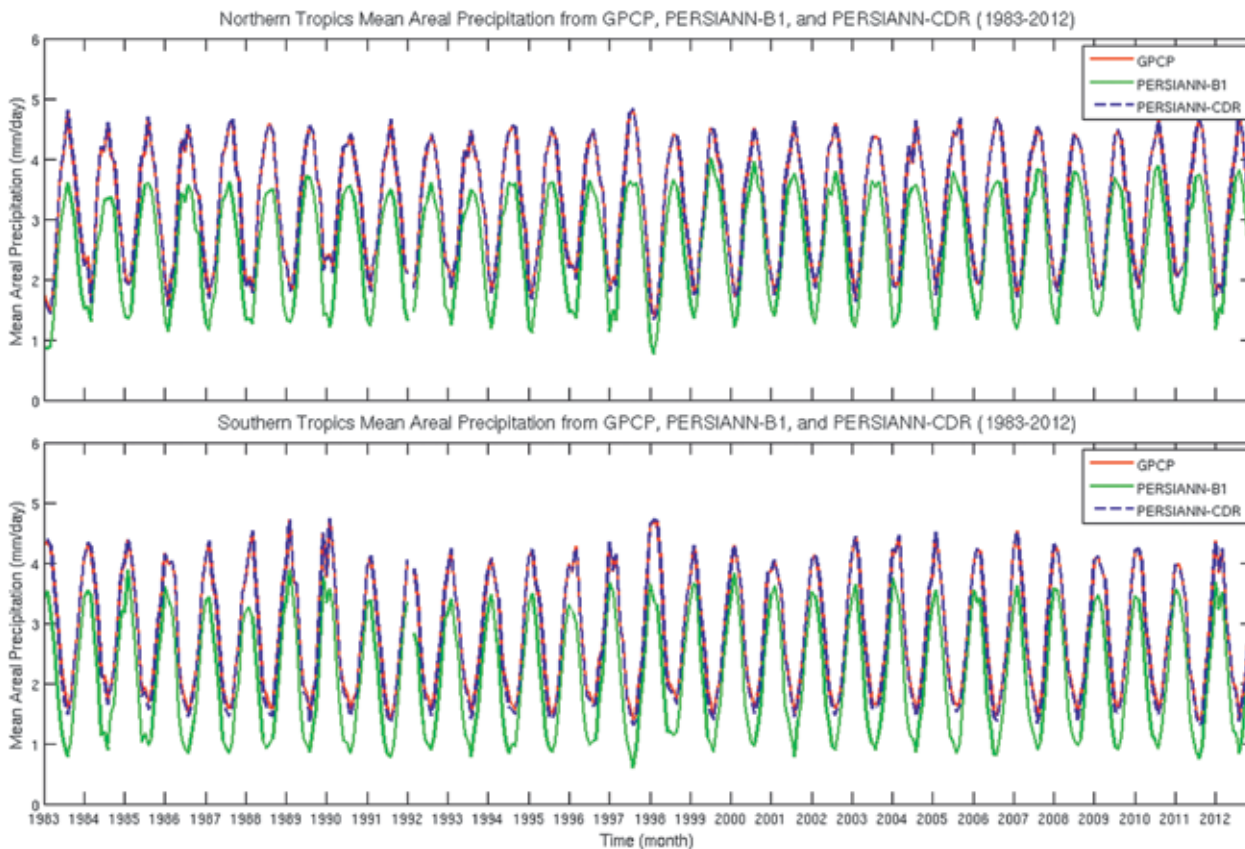

FIG. 3. Mean areal precipitation (mm day⁻¹) for (top) northern (0°–30°N) and (bottom) southern (0°–30°S) tropics from monthly GPCP (red; Adler et al. 2003), PERSIANN-B1 (green), and PERSIANN-CDR (dashed blue) datasets.
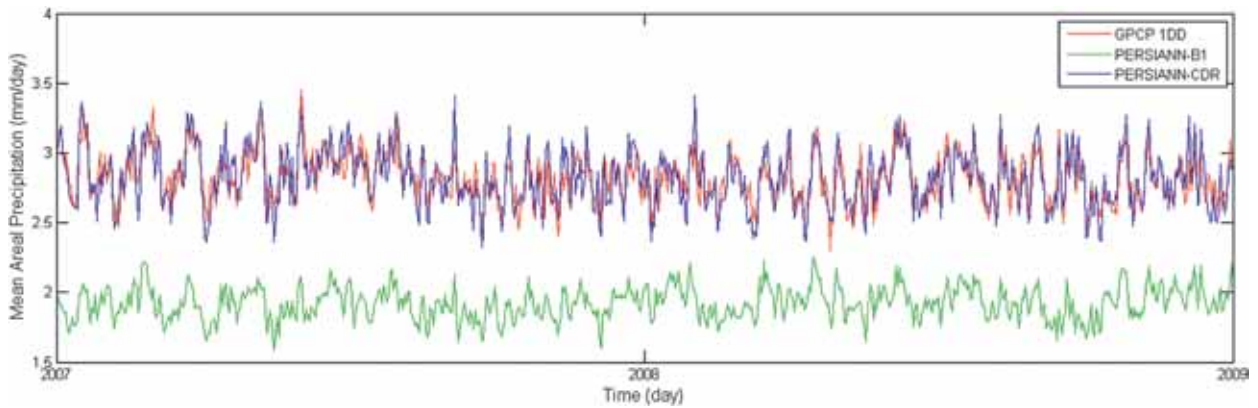
Fig. 4. Daily global (60°S–60°N) mean areal precipitation (mm day⁻¹) for the period of 2007–09 for GPCP-1DD (red; Huffman et al. 2001), PERSIANN-B1 (green), and PERSIANN-CDR (blue).
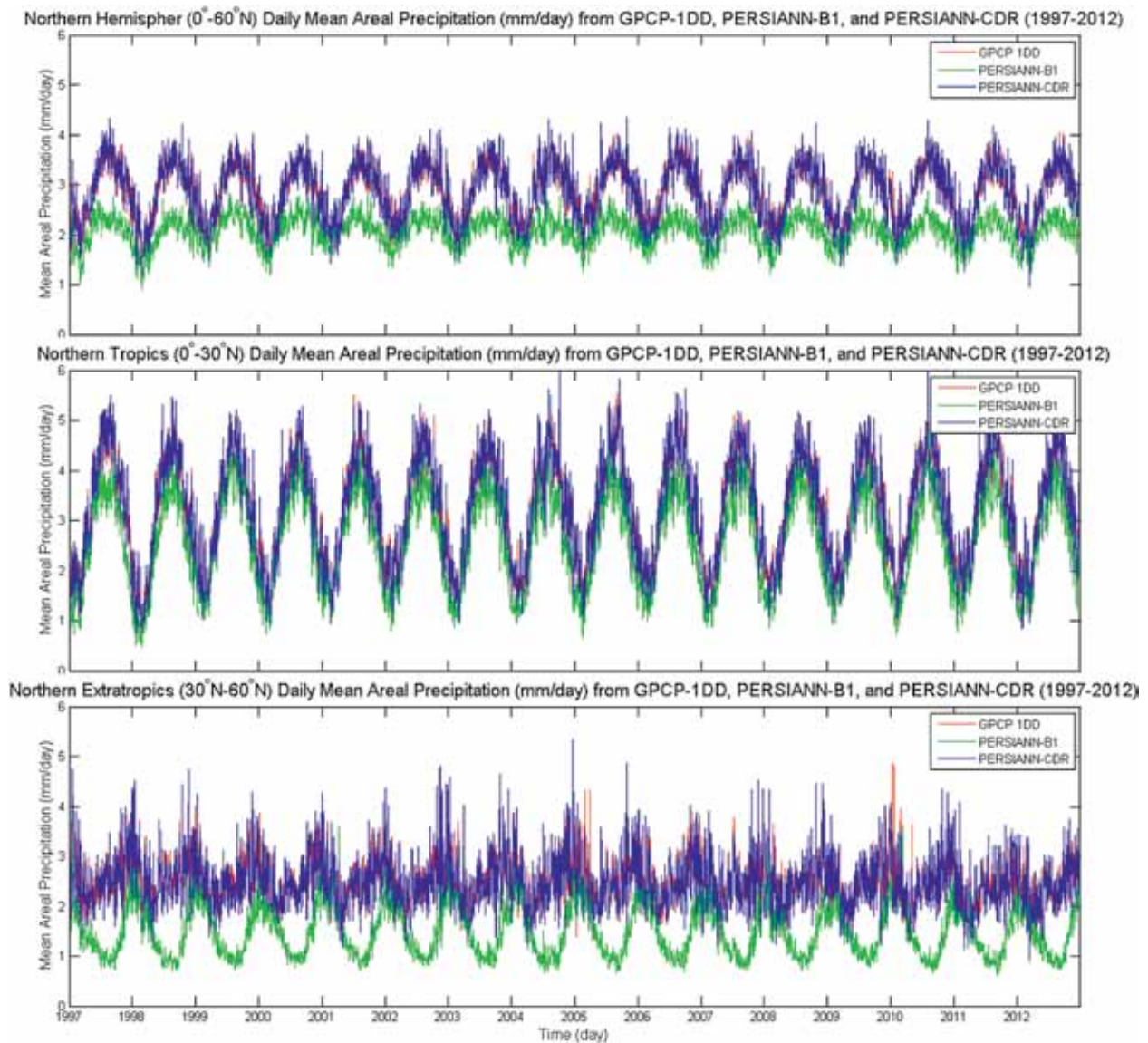

Fig. 5. Daily mean areal precipitation (mm day⁻¹) for the (top) Northern Hemisphere (0°–60°N) and northern (middle) tropics (0°–30°N) and (bottom) extratropics (30°–60°N) for the period of 1997–2012 from GPCP-1DD (red; Huffman et al. 2001), PERSIANN-B1 (green), and PERSIANN-CDR (blue).

algorithm to PERSIANN-B1 estimates (green line, Fig. 4). It shows that PERSIANN-CDR performs well in estimating the same global precipitation as GPCP-1DD, which benefits from the incorporation of PMW information (such as SSM/I and SSMI/S) in its estimate. It is noteworthy that no PMW data are used in PERSIANN-CDR, except indirectly from GPCP monthly data. Similar graphs for the Northern Hemisphere (0°–60°N) and the northern tropics (0°–30°N) and extratropics (30°–60N°) for the period of 1997–2012 are displayed in Fig. 5. As shown, even without any GPCP adjustment, the PERSIANN-B1 rain-rate estimates show good agreement with GPCP 1DD in tropical regions. The per-formance of PERSIANN-B1 over extratropical regions is poorer. In these regions, PERSIANN-B1 underes-timates the precipitation. However, after applying the GPCP bias adjustment, PERSIANN-CDR captures the precipitation patterns and demonstrates consider-able consistency with both GPCP daily and monthly precipitation products. The results are similar for the Southern Hemisphere (0°–60°S) and southern tropics (0°–30°S) and extratropics (30°–60S°).

FIG. 6. Top 5% heavy rainfall (mm day^{-1}) maps from (top) GPCP-1DD (Huffman et al. 2001), (middle) PERSIANN-CDR 1°, and (bottom) PERSIANN-CDR 0.25° for the period of 1997–2012.

To examine the performance of PERSIANN-CDR in the case of extreme precipitation events, the top 5% heavy rainfall (mm day^{-1}) patterns from GPCP-1DD (Fig. 6, top), PERSIANN-CDR upscaled to 1° (Fig. 6, middle), and PERSIANN-CDR 0.25° (Fig. 6, bottom) for the period of 1997–2012 are extracted. As shown in Fig. 6, the global patterns of extreme precipitation events are closely similar. PERSIANN-CDR depicts larger rainfall for some extreme precipitation events,
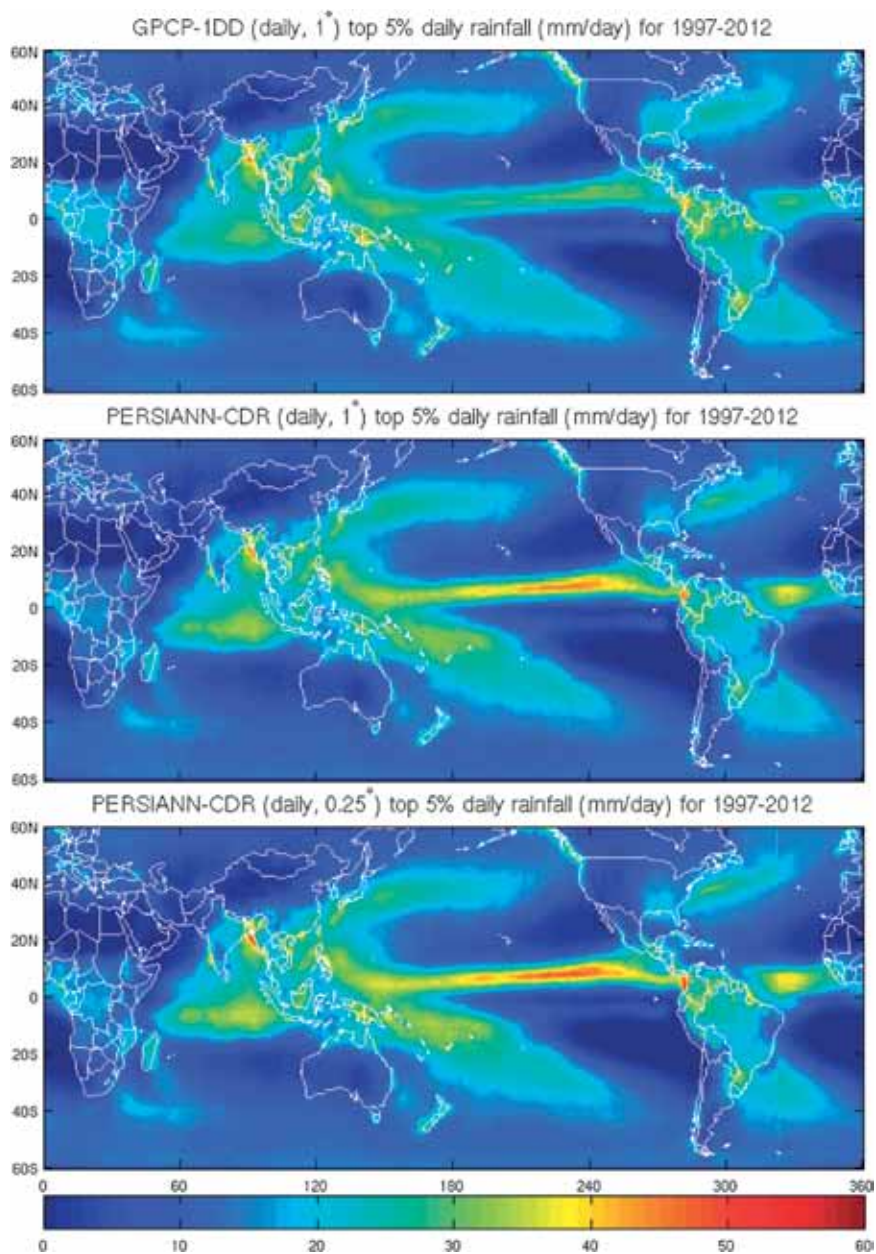
particularly over the intertropical convergence zone (ITCZ). Some of the observable differences are due to the spatial resolution differences between the two products, as extremes are smoothed and their intensity dampened in coarser resolution. This results in less intense extremes in the GPCP-1DD when compared to PERSIANN-CDR. Determining which of these two products is closer to the truth cannot be fully tested because of the lack of available measurements over the oceans. With the 0.25° rain-fall data from PERSIANN-CDR (Fig. 6, bottom), the

distribution of extremes can be seen at a finer resolution. These results show that the PERSIANN-CDR precipitation dataset has high potential to be a useful product for long-term climate studies at a much finer time scale than previously available.

CASE STUDIES. To investigate the performance of PERSIANN-CDR with respect to ground-truth and radar data, the following verification studies have been done. The first case study is related to the Hurricane Katrina in 2005 using the gauge-adjusted stage IV radar data. The second case study targets the pre-1997 period when current high-resolution satellite-based precipitation products were not available. It focuses on a major flood event over Sydney, Australia, in 1986, using the gridded daily gauge data provided by the Australia's Bureau of Meteorology. The third case study shows the comparison of the probability density function of PERSIANN-CDR with gauge observations and TMPA v7 over the contiguous United States (CONUS). Detailed descriptions follow.

Hurricane Katrina. Katrina occurred in August 2005 and is considered the most costly extreme weather event ever to strike the United States (Graumann et al. 2006). PERSIANN-CDR precipitation data

are compared with stage IV radar data at the 0.25° spatial scale during Hurricane Katrina. To examine the performance of PERSIANN-CDR with other satellite-based precipitation products, TMPA v7 was also included in the analysis. As shown in Fig. 7, PERSIANN-CDR (Fig. 7b) shows similar precipitation patterns to the radar data (Fig. 7c). Moreover, in regions where radars are blocked by mountains or a radar site is down (e.g., the Lake Charles radar site in southwest Louisiana during Katrina), the spatial coverage provided by PERSIANN-CDR is very valuable and captures a wide view of the precipitation and hurricane landfall.

The scatterplots of PERSIANN-B1, PERSIANN-CDR, and TMPA v7 against stage IV radar data are plotted and the relevant statistics are calculated. As shown in Fig. 8, the correlation coefficient between PERSIANN-B1 and radar data is significant (0.84), implying that even before doing any adjustment, PERSIANN-B1 is depicting similar patterns, albeit with lesser intensity (Fig. 7a) when compared to radar data (Fig. 7c). However, the RMSE (17.73) and bias (−0.4624) are rather large. After applying the GPCP adjustment
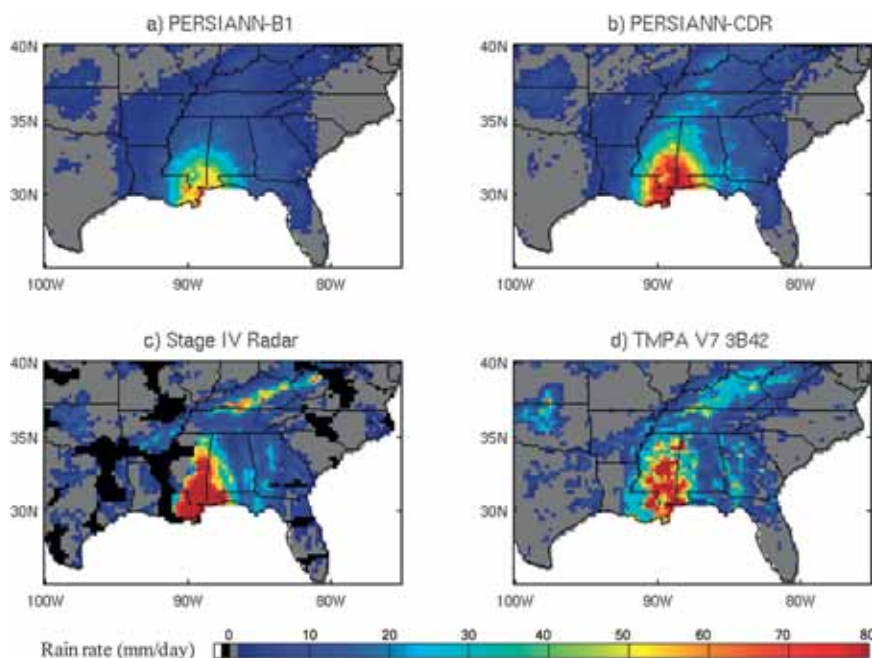

FIG. 7 (ABOVE). Rainfall (mm day⁻¹) over land during Hurricane Katrina on 29 Aug 2005 from (a) PERSIANN-B1, (b) PERSIANN-CDR, (c) stage IV radar (Lin and Mitchell 2005), and (d) TMPA v7 (Huffman et al. 2007). Black and gray pixels show radar blockages and zero precipitation, respectively.

FIG. 8 (RIGHT). Scatterplots of (top) PERSIANN-B1, (middle) PERSIANN-CDR, and (bottom) TMPA v7 (Huffman et al. 2007) against stage IV radar data (Lin and Mitchell 2005) for 29 Aug 2005 during Hurricane Katrina.
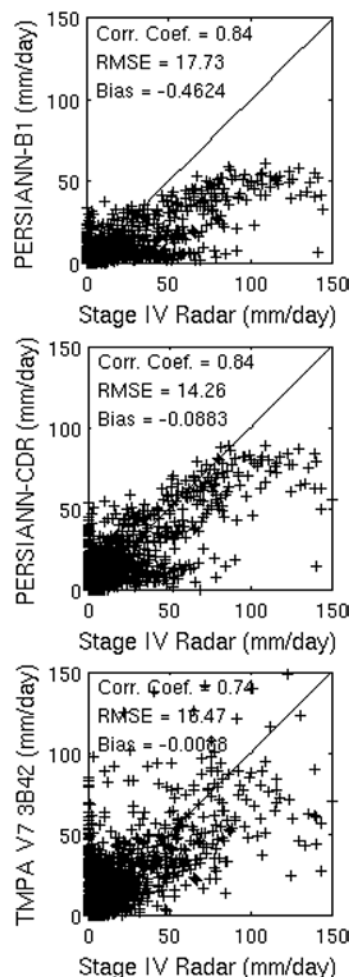
algorithm, the PERSIANN-CDR bias (−0.0883) is significantly reduced. PERSIANN-CDR and TMPA were each compared to stage IV radar data. As shown in Fig. 8, PERSIANN-CDR shows a higher correlation coefficient than TMPA; however, the bias in TMPA is lower than that in PERSIANN-CDR. These results show that each of the products have their respective strengths and shortcomings.

The 1986 Sydney flood. Sydney, Australia, experienced a historic flood from precipitation received on 5–6 August 1986, resulting in significant losses and disruptions to transportation systems (Handmer 1988). The performance of PERSIANN-CDR during this flood event was evaluated against interpolated daily rainfall gauge data from the Australian Bureau of Meteorology available at 0.05° spatial resolution (Jones et al. 2009). The 0.05° gridded data were resampled to 0.25° for compatibility with PERSIANN-CDR estimates. The rainfall maps from gauge data and PERSIANN-CDR, along with the respective scatterplot and statistics, are presented in Fig. 9. As shown, during the 1986 Sydney flood, PERSIANN-CDR shows a good correlation coefficient (0.62) with gauge data.

Regarding the observed differences in Fig. 9, besides uncertainties in PERSIANN-CDR and the sparsely distributed gauge network, some of the differences could be due to the temporal differences between the two datasets. PERSIANN-CDR daily grids correspond to a given 0000–2359 UTC time period; however, the Australian interpolated gauge data represent the 24-h accumulation of observations taken at 0900 local time (Jones et al. 2009). The local 0900–0900 daily rainfall accumulation in New South Wales and Victoria corresponds with 2300–2300 UTC. This is a 1-h difference from the PERSIANN-CDR daily grids. Therefore, for the case of Sydney flood presented in this study, the temporal differences probably do not contribute significantly to the rainfall differences but could be an issue in cases that cover larger areas and span from the east to the west with different local time. Such temporal inconsistencies in gauge observations may not be critical during dry seasons and drought years, but can introduce large differences in wet years, especially in cases of heavy rainfall events such as the August 1986 flood. In addition to the temporal

differences, since gauge data are point measurements, the interpolated product might not be able to represent the spatial coverage properly, which could also generate some significant differences between the satellite and gauge observations.
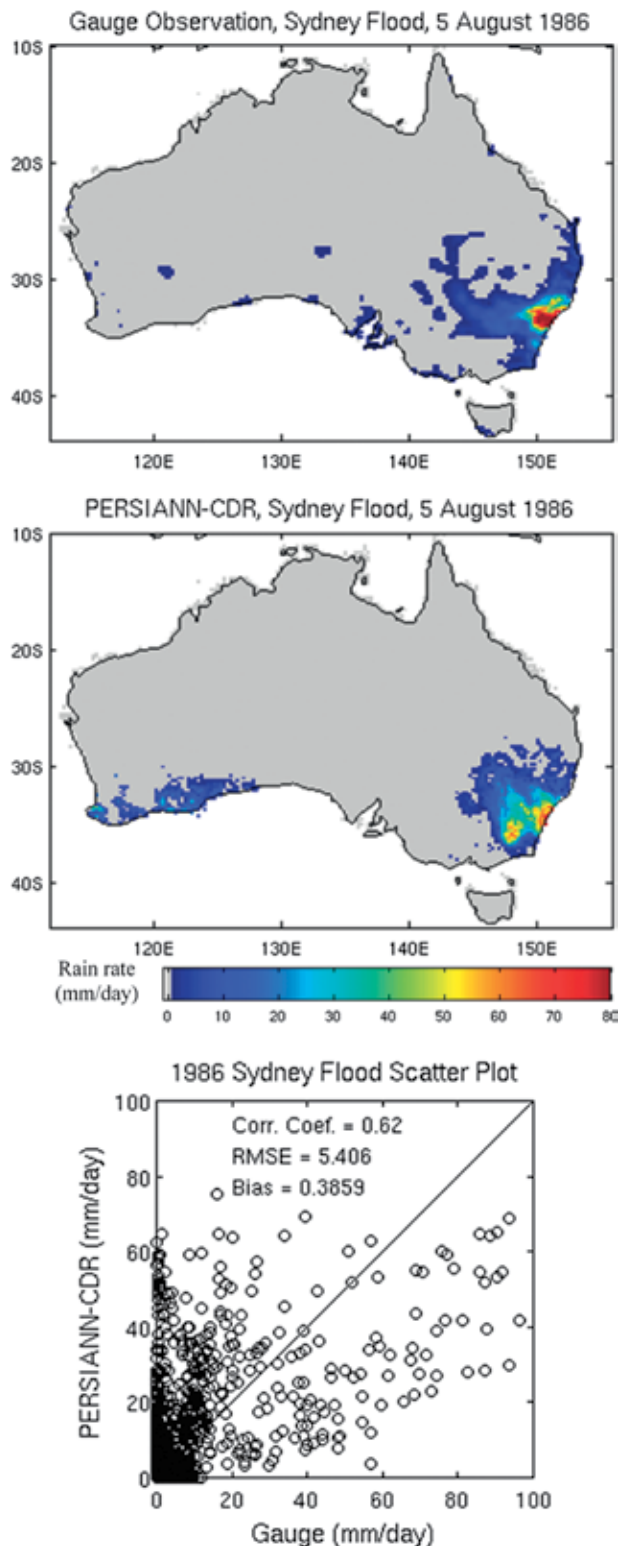

Fig. 9. Rainfall (mm day⁻¹) over land during the Sydney, Australia, flood on 5 Aug 1986 from (top) gauge observation (Jones et al. 2009) and (middle) PERSIANN-CDR rain-rate estimates. (bottom) The scatterplot and respective statistics.

Probability density function. For validation of PERSIANN-CDR, the probability density functions (PDFs) of PERSIANN-B1, PERSIANN-CDR, and TMPA v7 over CONUS for the period of 1998–2008 were extracted and compared. The CPC unified gauge-based analysis of daily precipitation over CONUS was included as a reference to compare the performance of other products. The CPC U.S. unified precipitation data are provided by the NOAA/Office of Oceanic and Atmospheric Research/Earth System Research Laboratory Physical Science Division (NOAA/OAR/ESRL PSD), Boulder, Colorado, from their website at www.esrl.noaa.gov/psd/data/gridded/data.unified .html (Higgins et al. 2000).

The empirical PDFs of these products are plotted and shown in Fig. 10. As shown, the PERSIANN-B1 PDF moves toward the CPC Gauge PDF after applying the bias-adjustment algorithm. Comparing the PDFs of TMPA and PERSIANN-CDR with the PDF of CPC gauge data indicates that both of these satellite-derived precipitation products are doing a reasonable job of matching CPC gauge PDF, although they both overestimate or underestimate the probability for some precipitation ranges.

CONCLUSIONS. A 30-yr period, daily, 0.25°, near-global satellite-based precipitation product, named PERSIANN-CDR, is developed and introduced in this paper. As a high-resolution satellite-based dataset, PERSIANN-CDR provides time series of precipitation of sufficient length, consistency, and continuity to study trends and observed changes in global and regional precipitation patterns due to climate change and natural variability. These characteristics are consistent with the CDR definition as described in the National Research Council (2004) report. The archives of historical GridSat-B1 IRWIN data are used in the PERSIANN model to produce historical rainfall estimates. These estimates are then bias corrected with the GPCP 2.5° monthly data, which include the GPCC gauge information. Consistency of PERSIANN-CDR is an important criterion that is maintained throughout the entire process.

The performance of PERSIANN-CDR is tested and reported for three case studies. The first study is for Hurricane Katrina (2005) as a precipitation event in more recent years for which better ground-based observations (such as gauge-adjusted stage IV radar data) and other high-resolution satellite products are available for comparison purposes. The second study captures the Sydney, Australia, flood event back in 1986 when other high-resolution precipitation products did not provide rainfall information. For these two studies, the results show that PERSIANN-CDR is performing reasonably well when compared to radar and ground-based observations. The third study examines the frequency distribution of precipitation from PERSIANN-CDR as compared to those of CPC gauge observations and TMPA v7. The results indicate that PERSIANN-CDR depicts a PDF similar to that of CPC gauge data, although it generally tends to underestimate the frequency distribution. Such difference
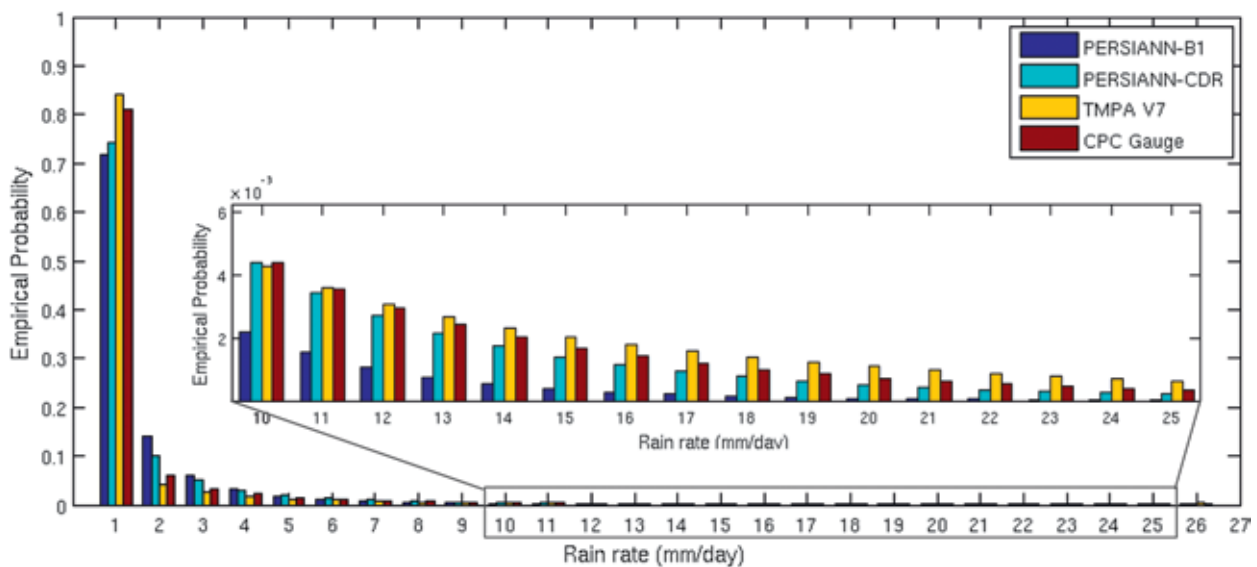

FIG. 10. Comparing the empirical PDF of PERSIANN-B1, PERSIANN-CDR, TMPA V7 (Huffman et al. 2007), and CPC unified gauge-based analysis of daily precipitation (Higgins et al. 2000) over the CONUS during the period of 1998–2008.

could be due to both the uncertainties in this product and/or the sparseness of the gauge network as well as the uncertainties associated with interpolation methods. The frequency distribution of PERSIANN-CDR was also compared with that of TMPA v7. Despite the expected and exhibited differences with each other and also when compared to CPC gauge data, both products seem to show similar patterns.

PERSIANN-CDR should prove to be a useful dataset for addressing various key climatological and hydrological research questions that require longer and finer resolution (daily, 0.25°) data than previously available. The PERSIANN-CDR product is available to the public as an operational climate data record on the NOAA NCDC CDR Program website under the atmospheric CDRs category (www.ncdc.noaa .gov/cdr/operationalcdrs.html). In addition, a brief description of PERSIANN-CDR along with various other PERSIANN products can be found on the Center for Hydrometeorology and Remote Sensing (CHRS) website at the University of California, Irvine (www.chrs.web.uci.edu/).

Finally, in an ideal situation, one hopes to provide a "perfect" and error-free dataset to the scientific and user communities. While this is an admirable goal to strive toward, achieving it is a difficult one. This is particularly true in the case of satellite-based products. Not only do the algorithms need continual enhancement and recalibration, but the raw data to be utilized as inputs to the algorithms need to be expanded (e.g., including more relevant spectral bands from LEO and GEO satellites) and be periodically reevaluated and quality controlled. Therefore, as is the case for any new environmental dataset, improving the efficacy and accuracy of PERSIANN-CDR will continue to be a work in progress. In this regard, while we have presented reasonably good results based on limited testing, more evaluation and verification over different regions and seasons will be desirable. The feedback from users of this dataset will be of immense value to the authors.

REFERENCES

Adler, R., and Coauthors, 2003: The version-2 Global Precipitation Climatology Project (GPCP) monthly precipitation analysis (1979–present). *J. Hydrometeor.,* **4,** 1147–1167, doi:10.1175/1525-7541(2003)0042.0.CO;2.

AghaKouchak, A., A. Behrangi, S. Sorooshian, K. Hsu, and E. Amitai, 2011: Evaluation of satellite-retrieved extreme precipitation rates across the central United States. *J. Geophys. Res.,* **116,** D02115, doi:10.1029/2010JD014741.

Allan, R. P., B. J. Soden, V. O. John, W. Ingram, and P. Good, 2010: Current changes in tropical precipitation. *Environ. Res. Lett.,* **5,** 025205, doi:10.1088/1748 -9326/5/2/025205.

Anagnostou, E. N., V. Maggioni, E. I. Nikolopoulos, T. Meskele, F. Hossain, and A. Papadopoulos, 2010: Benchmarking high-resolution global satellite rainfall products to radar and rain-gauge rainfall estimates. *IEEE Trans. Geosci. Remote Sens.,* **48,** 1667–1683, doi:10.1109/TGRS.2009.2034736.

Bourassa, M. A., and Coauthors, 2013: High-latitude ocean and sea ice surface fluxes: Challenges for climate research. *Bull. Amer. Meteor. Soc.,* **94,** 403–423, doi:10.1175/BAMS-D-11-00244.1.

Burroughs, W., 2003: *Climate into the 21st Century.* Cambridge University Press, 240 pp.

Ebert, E. E., J. E. Janowiak, and C. Kidd, 2007: Comparison of near-real-time precipitation estimates from satellite observations and numerical models. *Bull. Amer. Meteor. Soc.,* **88,** 47–64, doi:10.1175/ BAMS-88-1-47.

Fulton, R. A., J. P. Breidenbach, D. J. Seo, D. A. Miller, and T. O'Bannon, 1998: The WSR-88D rainfall algorithm. *Wea. Forecasting,* **13,** 377–395, doi:10.1175/1520-0434(1998)0132.0.CO;2.

Graumann, A., T. Houston, J. Lawrimore, D. Levinson, N. Lott, S. McCown, S. Stephens, and D. Wuertz, 2006: Hurricane Katrina: A climatological perspective: Preliminary report. Tech Rep. 2005-01, NOAA/ NESDIS, National Climatic Data Center, 27 pp. [Available online at www.ncdc.noaa.gov/oa/reports /tech-report-200501z.pdf.]

Gruber, A., and V. Levizzani, 2008: Assessment of global precipitation products. Tech. Rep. WRCP-128, WMO/TD-No. 1430, 55 pp. [Available online at www.gewex.org/reports/2008AssessmentGlobal PrecipReport.pdf.]

Habib, E., B. F. Larson, and J. Graschel, 2009: Validation of NEXRAD multisensory precipitation estimates using an experimental dense rain gauge network in south Louisiana. *J. Hydrol.,* **373,** 463–478, doi:10.1016/j.jhydrol.2009.05.010.

Handmer, J., 1988: The performance of the Sydney flood warning system, August 1986. *Disasters,* **12,** 37–49, doi:10.1111/j.1467-7717.1988.tb01153.x.

Higgins, R. W., W. Shi, E. Yarosh, and R. Joyce, 2000: Improved U.S. precipitation quality control system and analysis. NCEP/Climate Prediction Center Atlas 7, 40 pp.

——, V. B. S. Silva, W. Shi, and J. Larson, 2007: Relationships between climate variability and fluctuations in daily precipitation over the United States. *J. Climate,* **20,** 3561–3579, doi:10.1175/JCLI4196.1.

Hou, A., G. S. Jackson, C. Kummerow, and J. M. Shepherd, 2008: Global precipitation measurement. *Precipitation: Advances in Measurement, Estimation, and Prediction,* S. Michaelides, Ed., Springer, 131–170.

——, and Coauthors, 2014: The Global Precipitation Measurement Mission. *Bull. Amer. Meteor. Soc.,* **95,** 701–722, doi:10.1175/BAMS-D-13-00164.1.

Hsu, K., X. Gao, S. Sorooshian, and H. V. Gupta, 1997: Precipitation estimation from remotely sensed information using artificial neural networks. *J. Appl. Meteor. Climatol.,* **36,** 1176–1190, doi:10.1175/1520-0450(1997)0362.0.CO;2.

——, H. V. Gupta, X. Gao, and S. Sorooshian, 1999: Estimation of physical variables from multichannel remotely sensed imagery using a neural network: Application to rainfall estimation. *Water Resour. Res.,* **35,** 1605–1618, doi:10.1029/1999WR900032.

Huffman, G. J., and Coauthors, 1997: The Global Precipitation Climatology Project (GPCP) combined precipitation dataset. *Bull. Amer. Meteor. Soc.,* **78,** 5–20, doi:10.1175/1520-0477(1997)0782.0.CO;2.

——, R. F. Adler, M. M. Morrissey, D. T. Bolvin, S. Curtis, R. Joyce, B. McGavock, and J. Susskind, 2001: Global precipitation at one-degree daily resolution from multisatellite observations. *J. Hydrometeor.,* **2,** 36–50, doi:10.1175/1525-7541(2001)0022.0.CO;2.

——, and Coauthors, 2007: The TRMM Multisatellite Precipitation Analysis (TMPA): Quasi-global, multiyear, combined-sensor precipitation estimates at fine scales. *J. Hydrometeor.,* **8,** 38–55, doi:10.1175/JHM560.1.

——, R. F. Adler, D. T. Bolvin, and G. Gu, 2009: Improving the global precipitation record: GPCP version 2.1. *Geophys. Res. Lett.,* **36,** L17808, doi:10.1029/2009GL040000.

Janowiak, J. E., R. J. Joyce, and Y. Yarosh, 2001: A real-time global half-hourly pixel resolution IR dataset and its applications. *Bull. Amer. Meteor. Soc.,* **82,** 205–217, doi:10.1175/1520-0477(2001)0822.3.CO;2.

Jones, D. A., W. Wang, and R. Fawcett, 2009: High-quality spatial climate data-sets for Australia. *Aust. Meteor. Oceanogr. J.,* **58,** 233–248.

Joyce, R. J., J. E. Janowiak, P. A. Arkin, and P. Xie, 2004: CMORPH: A method that produces global precipitation estimates from passive microwave and infrared data at high spatial and temporal resolution. *J. Hydrometeor.,* **5,** 487–503, doi:10.1175/1525-7541(2004)0052.0.CO;2.

Karl, T. R., R. W. Knight, and N. Plummer, 1995: Trends in high-frequency climate variability in the twentieth century. *Nature,* **377,** 217–220, doi:10.1038/377217a0.

Knapp, K. R., 2008a: Scientific data stewardship of International Satellite Cloud Climatology Project B1 global geostationary observations. *J. Appl. Remote Sens.,* **2,** 023548, doi:10.1117/1.3043461.

——, 2008b: Calibration assessment of ISCCP geostationary infrared observations using HIRS. *J. Atmos. Oceanic Technol.,* **25,** 183–195, doi:10.1175/2007JTECHA910.1.

——, and Coauthors, 2011: Globally gridded satellite observations for climate studies. *Bull. Amer. Meteor. Soc.,* **92,** 893–907, doi:10.1175/2011BAMS3039.1.

Kucera, P. A., E. E. Ebert, F. J. Turk, V. Levizzani, D. Kirschbaum, F. J. Tapiador, A. Loew, and M. Borsche, 2013: Precipitation from space: Advancing Earth system science. *Bull. Amer. Meteor. Soc.,* **94,** 365–375, doi:10.1175/BAMS-D-11-00171.1.

Kummerow, C., W. Barnes, T. Kozu, J. Shiue, and J. Simpson, 1998: The Tropical Rainfall Measuring Mission (TRMM) sensor package. *J. Atmos. Oceanic Technol.,* **15,** 809–817, doi:10.1175/1520-0426(1998)0152.0.CO;2.

——, and Coauthors, 2000: The status of the Tropical Rainfall Measuring Mission (TRMM) after two years in orbit. *J. Appl. Meteor.,* **39,** 1965–1982, doi:10.1175/1520-0450(2001)0402.0.CO;2.

Lin, Y., and K. E. Mitchell, 2005: The NCEP stage II/IV hourly precipitation analyses: Development and applications. *Extended Abstracts, 19th Conf. on Hydrology,* San Diego, CA, Amer. Meteor. Soc., 1.2. [Available online at http://ams.confex.com/ams/Annual2005/techprogram/paper_83847.htm.]

Ma, H.-Y., H. Xiao, C. R. Mechoso, and Y. Xue, 2013: Sensitivity of global tropical climate to land surface processes: Mean state and interannual variability. *J. Climate,* **26,** 1818–1837, doi:10.1175/JCLI-D-12-00142.1.

Maddox, R. A., J. Zhang, J. J. Gourley, and K. W. Howard, 2002: Weather radar coverage over the contiguous United States. *Wea. Forecasting,* **17,** 927–934, doi:10.1175/1520-0434(2002)0172.0.CO;2.

National Research Council, 2004: *Climate Data Records from Environmental Satellites: Interim Report.* The National Academies Press, 150 pp.

Peterson, T. C., P. A. Stott, and S. Herring, Eds., 2012: Explaining extreme events of 2011 from a climate perspective. *Bull. Amer. Meteor. Soc., 93,* 1041–1067, doi:10.1175/BAMS-D-12-00021.1.

Rossow, W. B., and R. A. Schiffer, 1991: ISCCP cloud data products. *Bull. Amer. Meteor. Soc., 72,* 2–20, doi:10.1175/1520-0477(1991)0722.0.CO;2.

——, and L. C. Garder, 1993: Cloud detection using satellite measurements of infrared and visible radiances for ISCCP. *J. Climate, 6,* 2341–2369, doi:10.1175/1520-0442(1993)0062.0.CO;2.

——, A. Mekonnen, C. Pearl, and W. Goncalves, 2013: Tropical precipitation extremes. *J. Climate, 26,* 1457–1466, doi:10.1175/JCLI-D-11-00725.1.

Rudolf, B., 1993: Management and analysis of precipitation data on a routine basis. *Proc. Int. WMO/IAHS/ETH Symp. on Precipitation and Evaporation,* Bratislava, Slovakia, Slovak Hydrometeorological Institute, 69–76.

——, H. Hauschild, W. Rueth, and U. Schneider, 1994: Terrestrial precipitation analysis: Operational method and required density of point measurements. *Global Precipitation and Climate Change,* M. Desbois and F. Desalmond, Eds., Springer-Verlag, 173–186.

Schneider, U., A. Becker, T. Fuchs, A. Meyer-Christoffer, and B. Rudolf, 2008: Global precipitation analysis products of the GPCC. Deutscher Wetterdienst, 12 pp. [Available online at ftp://ftp-anon.dwd.de/pub/data/gpcc/PDF/GPCC_intro_products_2008.pdf.]

Simpson, J., R. F. Adler, and G. R. North, 1988: A proposed Tropical Rainfall Measuring Mission (TRMM) satellite. *Bull. Amer. Meteor. Soc., 69,* 278–295, doi:10.1175/1520-0477(1988)0692.0.CO;2.

Solomon, S., D. Qin, M. Manning, Z. Chen, M. Marquis, K. B. Averyt, M. Tigora, and H. L. Miller, Eds., 2007: *Climate Change 2007: The Physical Science Basis.* Cambridge University Press, 996 pp.

Sorooshian, S., K.-L. Hsu, X. Gao, H. V. Gupta, B. Imam, and D. Braithwaite, 2000: Evaluation of PERSIANN system satellite-based estimates of tropical rainfall. *Bull. Amer. Meteor. Soc., 81,* 2035–2046, doi:10.1175/1520-0477(2000)0812.3.CO;2.

Turk, J. T., G. V. Mostovoy, and V. Anantharaj, 2010: The NRL-Blend high resolution precipitation product and its application to land surface hydrology. *Satellite Rainfall Applications for Surface Hydrology,* M. Gebremichael and F. Hossain, Eds., Springer, 85–104, doi:10.1007/978-90-481-2915-7_6.

WCRP, 1986: Report of the workshop on global large scale precipitation data sets for the World Climate Research Programme. WCP-111, WMO/TD-No. 94, 45 pp.

Wentz, F. J., L. Ricciardulli, K. Hilburn, and C. Mears, 2007: How much more rain will global warming bring? *Science, 317,* 233–235, doi:10.1126/science.1140746.

Westrick, K. J., C. F. Mass, and B. A. Colle, 1999: The limitations of the WSR-88D radar network for quantitative precipitation measurement over the coastal western United States. *Bull. Amer. Meteor. Soc., 80,* 2289–2298, doi:10.1175/1520-0477(1999)0802.0.CO;2.

Xie, P., and P. A. Arkin, 1997: Global precipitation: A 17-year monthly analysis based on gauge observations, satellite estimates, and numerical model outputs. *Bull. Amer. Meteor. Soc., 78,* 2539–2558, doi:10.1175/1520-0477(1997)0782.0.CO;2.

——, J. E. Janowiak, P. A. Arkin, R. Adler, A. Gruber, R. Ferraro, G. J. Huffman, and S. Curtis, 2003: GPCP pentad precipitation analyses: An experimental dataset based on gauge observations and satellite estimates. *J. Climate, 16,* 2197–2214, doi:10.1175/2769.1.

Yilmaz, M. T., and T. DelSole, 2010: Predictability of seasonal precipitation using joint probabilities. *J. Hydrometeor., 11,* 533–541, doi:10.1175/2009JHM1187.1.

Young, C. B., and N. A. Brusnell, 2008: Evaluating NEXRAD estimates for the Missouri River Basin: Analysis using daily raingauge data. *J. Hydrol. Eng., 13,* 549–553, doi:10.1061/(ASCE)1084-0699(2008)13:7(549).

——, A. A. Bradley, W. F. Krajewki, A. Kruger, and M. Morrissey, 2000: Evaluating NEXRAD multisensory precipitation estimates for operational hydrologic forecasting. *J. Hydrometeor., 1,* 241–254, doi:10.1175/1525-7541(2000)0012.0.CO;2.

Zeweldi, D. A., and M. Gebremichael, 2009: Evaluation of CMORPH precipitation products at fine space–time scales. *J. Hydrometeor., 10,* 300–307, doi:10.1175/2008JHM1041.1.nn